Adaptive Dictionary Reconstruction for Compressed Sensing of ECG Signals

Darren Craven, *Student Member, IEEE*, Brian McGinley, Liam Kilmartin, *Member, IEEE*, Martin Glavin, *Member, IEEE*, and Edward Jones, *Senior Member, IEEE*

***Abstract*—This paper proposes a novel adaptive dictionary (AD) reconstruction scheme to improve the performance of compressed sensing (CS) with electrocardiogram signals (ECG). The method is based on the use of multiple dictionaries, created using dictionary learning (DL) techniques for CS signal reconstruction. The modified reconstruction framework is a two-stage process that leverages information about the signal from an initial signal reconstruction stage. By identifying whether a QRS complex is present and if so, determining a location estimate of the QRS, the most appropriate dictionary is selected and a second stage more refined signal reconstruction can be obtained. The performance of the proposed algorithm is compared with state-of-the-art CS implementations in the literature, as well as the set partitioning in hierarchical trees (SPIHT) wavelet-based lossy compression algorithm. The results indicate that the proposed reconstruction scheme outperforms all existing CS implementations in terms of signal fidelity at each compression ratio tested. The performance of the proposed approach also compares favorably with SPIHT in terms of signal reconstruction quality. Furthermore, an analysis of the overall power consumption of the proposed ECG compression framework as would be used in a body area network (BAN) demonstrates positive results for the proposed CS approach when compared with existing CS techniques and SPIHT.**

***Index Terms*—Compressed sensing (CS), dictionary learning (DL), electrocardiogram (ECG) compression, wireless body area networks (BANs).**

I. Introduction

RECENT years have seen a significant increase in the implementation of wireless body area networks (BANs). BANs enable continuous patient monitoring both in and out of a clinical environment, ultimately leading to the goal of pervasive healthcare. A major technical challenge to the realization of long-term ubiquitous monitoring BANs is minimizing the energy costs associated with wireless transmission [1], [2]. Therefore, a data reduction process in the form of lossy compression is useful to alleviate the impact of wireless transmission.

Manuscript received August 19, 2015; revised December 21, 2015 and February 10, 2016; accepted February 12, 2016. Date of publication February 18, 2016; date of current version May 3, 2017. This work was supported by the Higher Education Authority (HEA) under the Program for Research in Third Level Institutions (PRTLI) and the Irish Research Council (IRC).

The authors are with the College of Engineering and Informatics, National University of Ireland, Galway, Ireland (e-mail: d.craven1@nuigalway.ie; brianmcginley@gmail.com; liam.kilmartin@nuigalway.ie; martin.glavin@nuigalway.ie; edward.jones@nuigalway.ie).

Digital Object Identifier 10.1109/JBHI.2016.2531182

The primary goal of lossy compression is to provide minimal loss in signal fidelity while maximizing the compression ratio (*CR*). It is also important that the compression process is efficiently performed to ensure that it does not overly impact on the computational complexity of the implementation. Compressed sensing (CS) [3]–[5] is a low-energy compression approach that is considered promising for use in wireless BANs [6], [7]. The theory of CS is based on exploiting sparse representations of a signal in a particular dictionary. This has the benefit of offering low complexity data collection at a sub-Nyquist rate. In contrast, traditional state-of-the-art lossy compression algorithms generally employ Nyquist rate sampling followed by digitally implemented signal processing operations for compression. Examples of such Nyquist-based methods include the embedded zerotree wavelet (EZW) [8] and set partitioning in hierarchical trees (SPIHT) [9] algorithms. These wavelet-based techniques outperform CS in terms of signal reconstruction quality, however, they have an associated implementation cost that allow CS to compete in terms of overall system energy consumption [6].

The application of CS to electrocardiogram (ECG) compression has seen significant advancements recently in the areas of sampling, encoding, and reconstruction algorithms. In acquisition and encoding, Mamaghanian *et al.* proposed a sampling architecture that consumes 43% less energy than Nyquist rate sampling when applied to ECG signals [7] and also investigated strategies of combining redundancy removal and Huffman encoding to improve compression performance [6]. In terms of reconstruction, Zhang *et al*. [10] introduced the use of block-sparse Bayesian learning (BSBL) to reconstruct raw fetal ECG signals. The method leverages the intrablock correlation that exists in the sparsity pattern of wavelet coefficients in time domain fetal ECG signals, and then, uses BSBL in the reconstruction. Polania *et al.* [11] modified two reconstruction algorithms for CS with ECG signals: iterative hard thresholding (IHT) and compressive sampling matching pursuit (CoSAMP). Their modified model-based approaches (MMB-IHT and MMB-CoSAMP) utilize prior knowledge of signal structure to enhance reconstruction [11]. The two key attributes of their MMB approaches to CS is that the algorithms exploit both the high common support between the wavelet coefficients of consecutive ECG frames and the connected subtree structure formed by the largest coefficients across different scales in the wavelet transform output. Previous work by the authors investigated the use of patient specific dictionaries for CS-based ECG compression [12]. These dictionaries are created using

dictionary learning (DL) techniques and aim to exploit the highly structured nature of ECG signals.

Despite this progress, the aforementioned CS implementations, to date, remain outperformed by the most effective transform-based compression techniques such as SPIHT when commonly used energy-based distortion metrics such as percent root-mean-squared difference (*PRD*) are analyzed [11], [13]. This stimulates interest in new CS-based strategies that can improve performance in terms of distortion compared to algorithms such as SPIHT, while providing energy-efficiency advantages afforded by CS compared to Nyquist-rate approaches.

The first major contribution of this paper is a novel CS reconstruction framework based on an adaptive dictionary (AD) scheme. The proposed approach leverages knowledge of the signal based on an initial reconstruction pass with a standard learned dictionary. This signal information allows the reconstruction scheme to select a more suitable dictionary allowing for a second-stage refinement signal reconstruction pass. In conjunction with an analysis on signal reconstruction quality, a second major contribution to the paper is a detailed power comparison between the proposed CS technique, state-of-the-art CS implementations, and SPIHT. The power profiles were created by considering i) recent encoding techniques in the literature, ii) the power consumption of digital signal compression using an Analog Devices Blackfin DSP processor (BF537) as an example platform [14], and iii) wireless transmission via Bluetooth low energy (BLE) using a Texas Instruments CC2540 BLE transceiver [15]. The results demonstrate the ability of the proposed AD technique to outperform existing CS reconstruction algorithms in terms of signal reconstruction fidelity, and outperform both current CS techniques and SPIHT from a power consumption perspective. The signal performance gap between SPIHT and CS is also reduced in terms of signal reconstruction quality, the main area that currently limits existing CS methods.

The remaining sections are organized as follows. Section II provides a background on CS and DL. Section III details the proposed CS architecture and the novel reconstruction framework. Section IV presents a summary of the benchmark CS and SPIHT compression algorithms and includes a description of the performance metrics used. The experimental results analyzing signal reconstruction quality and overall power consumption are presented in Section V. A discussion and a use case example are presented in Section VI and Section VII concludes this paper.

II. Background

A. Compressed Sensing

The theory of CS is well defined in the literature [3]–[5], [16], therefore, this section will only briefly outline the principles and mathematics underlying CS. Let $X \in \mathbb{R}^N$ be a time sampled ECG signal that has a sparse representation in a dictionary $X = \Psi\alpha$. It then follows that $X = \Psi\alpha$, where α is the sparse vector representing the coefficients of the basis components. The basic CS sampling model measures compressed data $Y \in \mathbb{R}^M$, through linear combinations of X with a random sensing matrix $\Phi \in \mathbb{R}^{M \times N}$, such that $Y = \Phi X$, where $M \ll N$.

CS recovery involves solving the convex optimization problem in (1). In this paper, the sparse optimization is solved using the basis pursuit (BP) algorithm [17], where the sparse vector with the minimum l_1 norm will provide a close approximation to the original signal X, provided that enough measurements M have been taken.

$$\min_{\alpha \in \mathbb{R}^N} \|\alpha\|_1 \text{ subject to } Y = \Phi\Psi\alpha. \tag{1}$$

Once the sparse representation α is solved, X can then be reconstructed using $X = \Psi\alpha$. There are important conditions that Φ must satisfy to ensure accuracy and robustness in the signal recovery: *mutual coherence* with the sparse dictionary [18], the *null space property* [5], and the *restricted isometry property* [16].

B. Dictionary Learning

There are limitations associated with the use of standard orthogonal wavelet basis for CS-based reconstruction, particularly for a decreasing number of compressed measurements M [13]. Therefore, the use of overcomplete dictionaries created with data-driven DL techniques has previously been explored with CS [12], [19].

Given a set of t training signals $X_T = [X_1, X_2, X_3 \ldots X_t] \in \mathbb{R}^{N \times t}$ the objective of DL is to find an optimal dictionary $\Psi \in \mathbb{R}^{N \times P}$ that achieves sparse representations of the training signals in a set of coefficients $\beta \in \mathbb{R}^{P \times t}$. The dictionary Ψ is defined as being overcomplete when $P > N$.

In general, the aim of a DL algorithm is to iteratively improve the dictionary Ψ by achieving sparser representations of the training signals X_T and updating the dictionary based on the current sparse representations β. The common method for constructing the dictionary solves the optimization problem

$$\begin{aligned} &\min_{\Psi,\beta} \{||X_{TN,t} - \Psi_{N,P}\beta_{P,t}||_F\} \\ &\text{subject to } \|\beta_i\|_0 < S (i = 1, \ldots, K) \end{aligned} \tag{2}$$

where $||.||_F$ is the Frobenius norm and the process is bound by a sparsity constraint, such that the sparsity level S ensures that K is the maximum number of nonzero entries in each sparse representation β. In this paper, the dictionaries were created using the K-SVD algorithm proposed by Aharon *et al.* [20].

III. Proposed CS Approach

A. Acquisition and Compression

The signal acquisition block consists of a spread spectrum random modulation pre-integrator (SRMPI) design proposed by Mamaghanian *et al.*, which has been shown to outperform an analog-to-digital converter (ADC) sampling at the Nyquist rate and existing CS encoder strategies in terms of energy consumption [7]. The SRMPI model consists of a Nyquist rate mixer and parallel channels of random demodulators based on a random modulator pre-integrator (RMPI) design originally proposed by Yoo *et al.* [21]. The main innovation of the SRMPI model is a single Nyquist rate mixer prior to the RMPI that allows the mixers in each channel to operate at sub-Nyquist rates. The function of the mixers is to demodulate the input signal X based on a pseudorandom sequence, representative of the measurement matrix Φ. In this study, Φ assumes values of ± 1 with equal probability, as implemented with SRMPI [8]. The use of such Bernoulli

distributed matrices are widely considered a good choice for a random sensing matrix and have been used in previous CS ECG implementations [6], [11], [12]. The output of the demodulation is then accumulated using a low-pass filter or integrator. This value is then passed into an ADC, which can sample at a sub-Nyquist rate resulting in the compressed vector *Y*.

The use of a fixed sensing matrix and the pseudoperiodic nature of ECG signals gives rise to significant redundancy existing in consecutive CS measurement vectors *Y* [6]. Therefore, strategies to remove the redundancy and ensure a lossless extension in *CR* are typically employed [6], [11]. Here, Mamaghanian *et al.*'s redundancy removal technique that exploits the nonuniform nature of adjacent ECG measurement vectors is used. The difference between two consecutive vectors is further processed and quantization is performed on the difference to extend *CR*. Since the difference vector contains values, which are normally distributed, Huffman encoding is employed as an entropy encoder for an additional increase in *CR* prior to transmission. A Huffman dictionary is created offline corresponding to the nonuniform nature of the difference values. A Huffman dictionary is created offline corresponding to the nonuniform nature of the difference values. The target wireless transmission protocol considered for this research is low-power BLE.

B. Novel Adaptive Dictionary Reconstruction

The proposed AD reconstruction framework aims to improve the performance of standard dictionary (SD) learning-based CS implementations. The proposed approach operates as follows. Suppose X_i is an initial reconstruction where a dictionary Ψ_i is used in the convex optimization operation. The process then exploits the knowledge of X_i to optimize signal reconstruction by allowing a more suitable dictionary to be selected based on two key signal characteristics of X_i.

The first signal property is based on whether a QRS complex is detected in the first stage signal estimate X_i. If no QRS complex is present in X_i, the second stage of the algorithm consists of signal reconstruction with a dictionary Ψ_{NQ}, specifically trained with signals containing no QRS complex, and therefore, can provide a better definition of the signal information in the signal region between QRS complexes. Second, we determine the location of the QRS complex if one is present in X_i. In this case, q subdictionaries are created $\Psi_Q = [\Psi_{Q1}, \Psi_{Q2}, \Psi_{Q3} \ldots \Psi_{Qq}]$. Each dictionary is created with training signals that contain QRS complexes across individual temporal windows within the frame, each containing *N*/*q* samples, shifted across the frame with no overlap between windows. For example, the set of training signals used to create the dictionary Ψ_{Q1} contain QRS complexes in the sample regions [1:*N*/*q*]. In general, this concept allows the signal reconstruction quality to be improved, as the chosen subdictionary is trained for sparse representations of signals where the majority of signal energy in the frame is concentrated on that location. Fig. 1 demonstrates an example of training signals used to create the dictionaries Ψ_i (a), Ψ_{NQ} (b), and Ψ_{Q2} (c) (with $q = 12$ and $N = 192$).

A description of the AD process is illustrated in Algorithm 1. There are a few practical considerations that are worthwhile to mention. The length of the ECG frame $N = 192$, to ensure a good balance between the number of frames containing QRS complexes and non-QRS complex frames. Ideally the number of subdictionaries q is maximized to allow a minimal window size and good resolution in terms of each QRS location. However, there must also be sufficient training signals to create high-performing overcomplete dictionaries. Preliminary testing of variations of q, found that $q = 12$ provides optimal performance for $N = 192$. The QRS detection per frame is based on the maximum absolute deviation from mean value ($d_{\max} = \left|\,|\max(X_i)| - \overline{X_i}\,\right|$), whereby if this value exceeds a threshold Q_{Thresh} determined during training of the

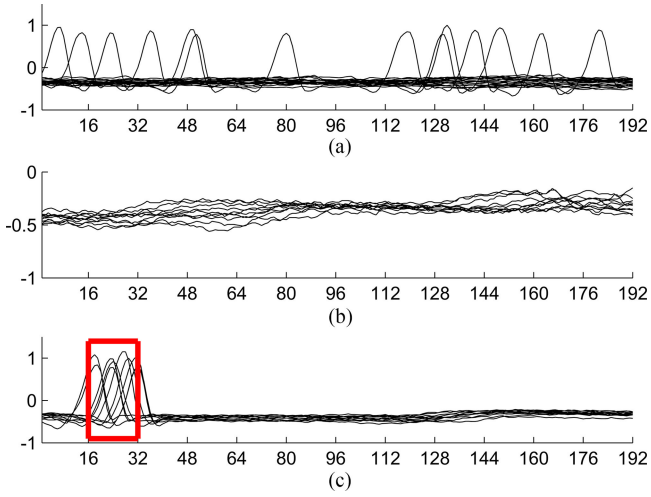

Fig. 1. Examples of 20 random training signals for various dictionary creations. (a) Standard DL approach where all types of signals are used in training to create Ψ_i. (b) Training frames for a subdictionary Ψ_{NQ} where no QRS complex is detected in a frame. (c) Training frames for a subdictionary Ψ_{Q2} where $q = 12$ and $N = 192$. The red box indicates the defined region where the QRS complex is present, for the training signals.

Algorithm 1: AD Reconstruction

Require: Compressed measurements *Y*, sensing matrix Φ, dictionaries Ψ_i, Ψ_{NQ}, and Ψ_{Q1}, Ψ_{Q2}, $\Psi_{Q3} \ldots \Psi_{Qq}$.
First Stage (SD):
$\min_{\alpha_i \in \mathbb{R}^N} ||\alpha_i||_1$ s.t. $Y = \Phi\Psi\alpha$
$X_i = \Psi_i \alpha_i$
Second Stage (AD):
$d_{\max} = \left|\,|\max(X_i)| - \overline{X_i}\,\right|$
if $(d_{\max} < Q_{\text{Thresh}})$ **then**
  $\min_{\alpha_{NQ} \in \mathbb{R}^N} ||\alpha_{NQ}||_1$ s.t. $Y = \Phi\Psi_{NQ}\alpha_{NQ}$
  $X' = \Psi_{NQ}\alpha_{NQ}$
else
  for $k = 1$ to N **do**
    if $\left|\,|(X_i(k))| - \overline{X_i}\,\right| = d_{\max}$ **then**
      $W = \text{round}(k/N + 0.5)$
      $\min_{\alpha_{QW} \in \mathbb{R}^N} ||\alpha_{QW}||_1$
      s.t. $Y = \Phi\Psi_{QW}\alpha_{QW}$
      $X' = \Psi_{QW}\alpha_{QW}$
return *X'*

dictionaries, the frame is deemed to contain a QRS complex. Generally QRS detection algorithms require more than $N = 192$ samples to accurately detect QRS locations and function by combining frames in such instances. A potential issue here is the occurrence of a QRS complex at the boundary between two frames. A QRS detection algorithm will correctly identify the sample location of the complex, however, the adjacent frame may still contain part of the QRS complex, and thus, a high-energy portion of the signal will remain. Using the maximum absolute deviation from mean ensures that if the amplitude of the portion of the complex contained per frame is above the threshold in accordance with training, it is treated as a QRS complex and this makes the algorithm more robust. A final note is that despite adding to the computational time of dictionary creation and doubling the reconstruction time compared to SD reconstruction, the proposed framework does not result in increased energy consumption in the actual sensors that constitute a BAN. This is because the reconstruction and dictionary creation are completed offline in an unconstrained power environment with no energy impact on the sampling, compression, or wireless transmission operations.

IV. Performance Evaluation

A. ECG Database

The ECG database used in these experiments was the MIT-BIH Arrhythmia database [22]. This database consists of 30-minute long patient records sampled at 360 Hz with 11-bit resolution. A subset of 11 patient records used in [11] and initially proposed by Lu *et al.* [23] were used. This database was chosen as it is widely used in the literature and it contains a variety of both routine and rare arrhythmia phenomenon, which makes it useful for clinical analysis. Furthermore, a MIT-BIH database directory [24] is provided that contains annotations of different physiological events in each record and this will provide a basis for visual assessment of reconstruction performance. As the target application is ambulatory ECG monitoring in a BAN, an additional MIT-BIH Noise Stress Test database will also be assessed [25]. The database contains increased levels of noise and morphologies such as baseline wander, electrode motion, and muscle artifacts. The ability of the proposed algorithm to maintain performance in such a testing scenario is, therefore, analyzed.

B. Patient Specific Training

Patient specific signals were used to create the Huffman dictionary (for encoding the redundancy removal output), the reconstruction dictionaries (using the K-SVD algorithm), and the QRS thresholds for the AD operation. Here, 50% of the records are used as training signals for the once-off training phase. The remaining 50% of the record not used during training were used for testing purposes. Dictionary creation was performed using a set of $t = 15000$ training signals X_T, with each overcomplete dictionary Ψ containing $P = 10000$ atoms.

The results were cross validated to ensure the complete patient records were used during testing and averaged over each record tested.

C. Benchmark Algorithms

In order to benchmark the performance of the proposed AD reconstruction scheme, the results are compared to those obtained with both the current state-of-the-art CS algorithms and the lossy compression method SPIHT.

1) State-of-the-Art CS Recovery Techniques: There are three main CS recovery techniques that will be used for comparison purposes to evaluate the AD framework. Previous work by the authors in [12] investigated the use of patient specific SD reconstruction with ECG signals. The results from the SD implementation will be used to highlight the improvements from utilizing the AD. While the SD technique relies on sparse representations during signal reconstruction, two alternative techniques that aim to exploit different structures in the wavelet coefficients of ECG signals are analyzed. Zhang *et al.*'s BSBL implementation [26] and the MMB approaches proposed by Polania *et al.* [11] are considered. The MMB method was compared with BSBL in [11] on the records used in these experiments and the results in [11] are, therefore, used for assessment in this paper. The MMB-IHT technique currently provides the best reported performance of CS-based ECG compression in the literature.

2) SPIHT: SPIHT is a lossy ECG compression technique proposed by Said and Pearlman [9]. The core principles of SPIHT are derived from the EZW technique, which exploits the fact that wavelet coefficients from different subbands exhibit a temporal relationship between each other. SPIHT coding effectively orders the output of the discrete wavelet transform (DWT) according to the significance of each coefficient by scanning the coefficients according to a threshold. For this application, the CDF 5/3 biorthogonal lifting-based integer wavelet transform was used. The wavelet is computationally efficient to implement due to the simplicity of the multiplication steps and the limited number of lifting steps required compared with other wavelets [27], [28]. The DWT was performed using eight levels of decomposition and SPIHT coding techniques were applied to the output of the DWT to construct a compressed binary stream. In order to achieve this encoding, SPIHT maintains the coefficients in lists and recursively performs sorting and refinement passes on these lists to encode the wavelet information. As the bits are encoded in order of significance, simple control of *CR* can be obtained by truncating the bit stream at a desired *CR*. A detailed description of the implementation used can be found in [23].

D. Performance Metrics

The metrics used to quantify the compression algorithms are *CR*, *PRD* and average power consumption.

1) Compression Ratio: *CR* is a measure of the data reduction required to represent the original signal. The frame size of the signals is *N*, B_O is the original bit resolution, which is 11 bits, and B_T is the number of transmitted bits per frame after Huffman coding. *CR* is defined as

$$CR = \frac{(N)(B_O)}{B_T}. \tag{3}$$

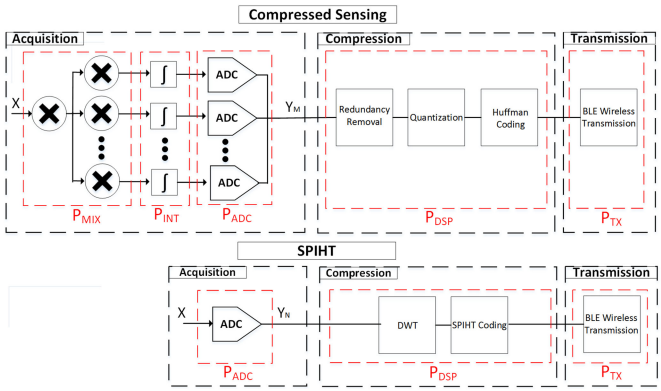

Fig. 2. Block diagrams for the acquisition, compression, and transmission operations for CS (top) and SPIHT (bottom). An SRMPI design is used for CS acquisition. SPIHT includes a Nyquist rate ADC. CS compression includes redundancy removal, quantization, and Huffman coding before BLE wireless transmission. SPIHT comprises a DWT and SPIHT coding before the binary stream is transmitted.

2) Percent Root-mean-squared Difference: *PRD* is a measurement of the distortion between the reconstructed signal *X'* and the original *X*. There are two common definitions of *PRD*

$$PRD = \frac{||X - X'||}{||X||}.100 \tag{4}$$

$$PRD^* = \frac{||X - X'||}{||X - \bar{X}||}.100. \tag{5}$$

With *PRD*, the mean of the signal $\bar{X}$ is not removed from the original signal. This can result in a DC bias artificially lowering the distortion results. PRD^* is, therefore, more commonly used, however, *PRD* is included for more direct comparison with CS implementations in the literature.

3) Power Consumption Models: The CS and SPIHT architectures assumed in this paper for acquisition, compression, and transmission are detailed in Fig. 2. The power consumption of each algorithm is determined by calculating the power required in i) sampling the signal, ii) performing digital signal compression on a Blackfin (BF537) DSP [14], and iii) wireless transmission of the ECG data using the Texas Instruments CC2540 BLE wireless transceiver [15]. The variables used in the power analysis are defined in Table I, and their values given. Each component of the power calculation is now treated in more detail.

a) Acquisition:

Mixer: Mamaghanian *et al.*'s [7] SRMPI design implemented mixers using the single pole, double throw CMOS switch (ADG636) from Analog Devices. The sub-Nyquist rate mixers were operating at half the Nyquist sampling frequency and a similar approach is utilized in this paper. The mixer power (P_{MIX}) is defined as

$$P_{\mathrm{MIX}} = (fs)\,(Mx) + (C)\left(\frac{fs}{2}\right)(Mx). \tag{6}$$

TABLE I
VARIABLES USED IN POWER CALCULATIONS

Variable	Value	Notes
fs	360 Hz	ECG sampling frequency [22]
B	11	ECG bit resolution [22]
N	–	ECG frame size (CS—192, SPIHT—1024)
V_{DD}	0.6 V	CS sampling integrator operating voltage [29]
Mx	0.2938 nJ	Mixer energy per CS conversion [7]
C	16	Number of SRMPI channels
Cp	10 fF	Integrator capacitance [29]
M	–	Number of compressed measurements.
FOM	10 fJ	*FOM* for ADCs per conversion [30]
I_{DD}	15 mA	Blackfin baseline dynamic current [31]
ASF	1	Blackfin activity scaling factor [31]
V_{BF}	0.8 V	Blackfin operating voltage [31]
AEC	–	Average execution cycle in VisualDSP++
CLK	100 MHz	Blackfin core clock frequency [31]
B_T	–	Number of bits transmitted per frame

Integrator: The integrator power estimation (P_{INT}) is taken from Chen *et al.*'s CS implementation [29].

$$P_{\mathrm{INT}} = \frac{(C)\left(Vdd^2\right)(10pi)\,(fs)\,(Cp)}{16}. \tag{7}$$

ADC: The SPIHT power model assumes Nyquist rate (*fs*) sampling. In contrast, the CS model effectively operates at a sub-Nyquist rate of (*fs*)(*M/N*). The figure-of-merit (*FOM*) is based on a recent survey of ADCs [30] that concluded the most energy efficient ADCs are successive approximation register ADCs, which can provide a *FOM* of <10 fJ per conversion. The ADC power for each algorithm (P_{ADC}) is then expressed as in (8). Note with SPIHT *M* is fixed and corresponds to the frame size *N*. For CS, *M* is alternating and is reduced as the *CR* increases.

$$P_{\mathrm{ADC}} = (M)\,(FOM)\left(2^B\right)(fs). \tag{8}$$

Overall Acquisition Power: The total power (P_{ACS} and P_{ASPIHT}) equations for each acquisition implementation (based on CS and SPIHT) are given as follows:

$$P_{\mathrm{ACS}} = P_{\mathrm{MIX}} + P_{\mathrm{INT}} + P_{\mathrm{ADC}} \tag{9}$$

$$P_{\mathrm{ASPIHT}} = P_{\mathrm{ADC}}. \tag{10}$$

b) Digital Signal Compression: The computational complexity of each compression algorithm is assessed by determining the average number of clock cycles to compress 1s of ECG data for each *CR* tested. The number of clock cycles was calculated for the Analog Devices Blackfin BF537 DSP using the Analog Devices Visual DSP++ code execution profiling tool.

The SPIHT implementation can be divided into two main processes: the DWT of the input signal and the SPIHT encoding operation. The CS implementation entails a redundancy removal operation, quantization, and Huffman coding. The Average Execution Cycle (*AEC*) count of each operation at different *CR*s was obtained and the power required (P_{DSP}) for each algorithm

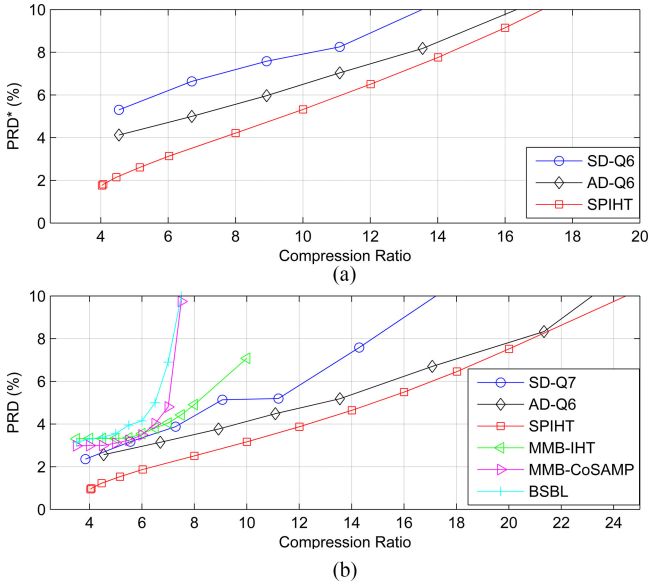

Fig. 3. (a) *PRD** and (b) *PRD* comparison between the SD and AD reconstruction approaches, the MMB-IHT and MMB-CoSAMP, and BSBL approaches in the literature and SPIHT. Q6 and Q7 indicate quantization of the difference values at 6 and 7 bits, respectively.

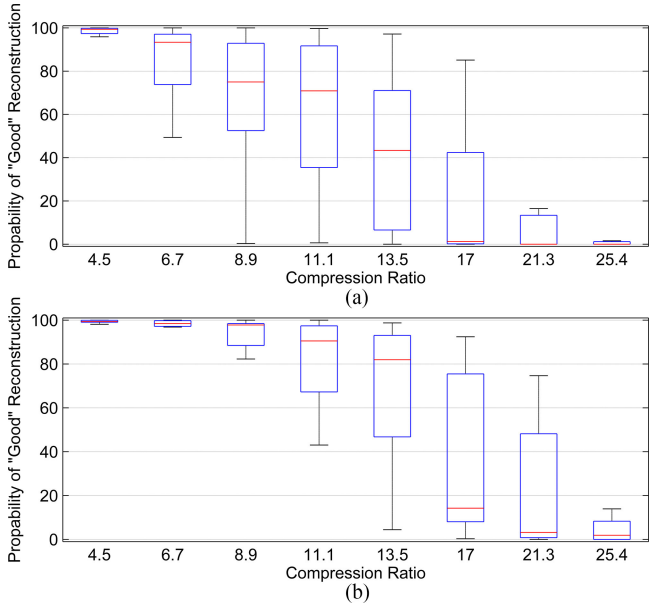

Fig. 4. Boxplots of (a) SD-Q6 and (b) AD-Q6 showing the probability of a "good" reconstruction.

was calculated as in follows, based on [31].

$$P_{\mathrm{DSP}} = (I_{\mathrm{DD}})\,(\mathrm{ASF})\,(V_{\mathrm{BF}})\left(\frac{\mathrm{AEC}}{\mathrm{CLK}}\right)\left(\frac{fs}{N}\right). \tag{11}$$

c) Wireless Transmission: Siekkinen *et al.* [32] measured the power consumption of a Texas Instruments CC2540 BLE transceiver [15] as 84 mW during wireless transmission. The recorded duration to transmit one byte of data was 8 μs. It can then be estimated the energy required to transmit one bit of data is 84 nJ using BLE. Therefore, the power consumed per transmission (P_{TX}) for each algorithm is dependent on the level of compression and is calculated as follows:

$$P_{TX} = (84nJ)\,(B_T)\left(\frac{fs}{N}\right). \tag{12}$$

V. Experimental Results

A. Signal Energy-Based Distortion

Fig. 3 (a) shows the average *PRD** of the proposed AD approach compared with SD reconstruction and SPIHT. AD-Q6 (i.e., the proposed technique with quantization of the difference values at 6 bits) outperforms the SD-Q6 reconstruction method across all *CR*s tested. While SPIHT still performs better than CS, the proposed technique reduces the gap in performance with SPIHT. Zigel *et al.* [33] assessed different *PRD** ranges and their suitability for clinical diagnosis as perceived by clinical specialists. Their results indicated that for values $< 9\%$ *PRD**, the signal reconstruction quality could be classified as "good." Therefore, in this analysis, a target *PRD** of 9% will be used as a basis for assessment of compression performance. At this *PRD** level, the AD approach extends the *CR* over the SD reconstruction from 12.1 to 14.8. SPIHT can achieve a *CR* of 15.9 for this *PRD** level.

The proposed AD-Q6, SD-Q7, SPIHT and the results presented in [11] for MMB-IHT, MMB-CoSAMP, and BSBL are compared in terms of *PRD* in Fig. 3 (b). It is clear AD-Q6 outperforms the MMB methods and BSBL for all *CR*s tested. The results in [11] only provide values for *PRD* over a range of *CR*s, and therefore, these results are shown here instead of *PRD**. However, this should not change our general conclusions in terms of comparison with these CS methods. While SPIHT still gives better overall performance, among the CS-based methods, the results obtained with the AD approach proposed here demonstrate a significant improvement in CS ECG implementations.

Boxplots for SD-Q6 (a) and AD-Q6 (b) show the probability of "good reconstruction" per 1024 samples averaged over all records in Fig. 4. In each box, the median is the central line, the box edges signify the 25th and 75th percentiles and the whiskers show the most extreme data points that are not considered outliers. It is clear from Fig. 4 that the AD improves the probability of "good" reconstruction. It also reduces the variance in reconstruction performance from record to record.

The MIT-BIH Arrhythmia database directory [24] provides annotations of the various beat types in each record. It is of great interest to monitor the performance of the compression algorithm in reconstructing different beats which differ from normal sinus heartbeats. For clinical diagnostics, it is important that the compression algorithm sufficiently preserves the information of these beats. Fig. 5 provides a visual evaluation of the measure of the ability of the AD method and SPIHT to preserve "good" signal reconstruction quality in the frames where two premature ventricular contraction (PVC) beats were annotated. This analysis is useful as it highlights the effectiveness of the

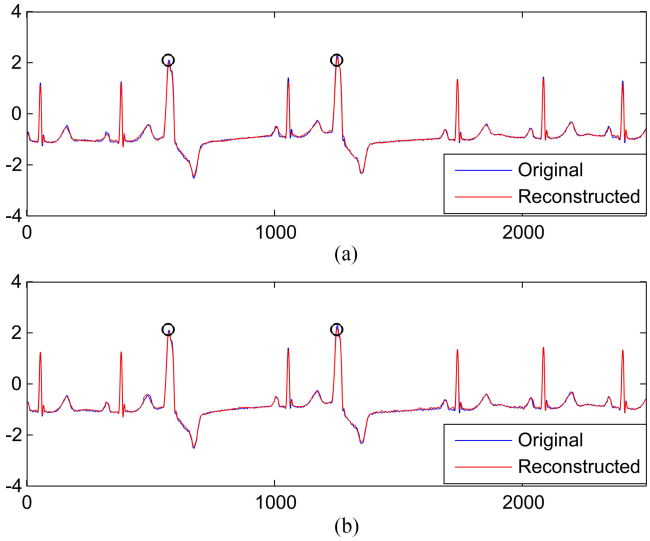

Fig. 5. Examples of two PVC events in record 119. The original signals are in blue and the reconstructed signals (with a $CR = 17.6$) are in red. (a) SPIHT reconstruction with a PRD^* of 7.05%; (b) AD reconstruction with a PRD^* of 6.66%. The black circle indicates the location of the annotated PVCs.

AD algorithm to reconstruct potential abnormal events in an ECG signal, providing similar reconstruction quality to SPIHT at a high *CR* of 17.6.

In order to further assess the potential of the proposed AD approach, the algorithm was tested on noisy ECG records typical of those recorded in a BAN environment. Physionet provides a noise stress test ECG database that contains baseline wander, muscle artifacts, and electrode motion artifacts [25]. These signals represent a more difficult testing scenario for the proposed algorithm. Noisy versions of two records (record 118 and 119) from the MIT-BIH Arrhythmia Database are provided, and therefore, results can be directly compared with the performance on the relatively "clean" ECG signal. The database provides 12 minutes of noisy ECG data per record. For the purposes of these experiments, noisy data at signal to noise ratio (*SNR*) levels of 24, 18, and 12 dB were extracted and used for dictionary creation and testing. Fig. 6 (b) and (c) shows reconstructed signals at 18 dB and 12 dB *SNR* levels. It is clear that the signals present more variability and a more difficult reconstruction problem for the proposed algorithm.

Due to the increased level of noise present, the signals were reconstructed with the BP Denoise algorithm, which is defined by the reconstruction problem in (13) [17], [34]. The BP Denoise algorithm is useful in scenarios where the signal is corrupted by noise. The bounding parameter σ balances the optimization between sparsity and signal reconstruction quality. For these experiments, we set the parameter $\sigma = 10^{-6}$ and increased the number of iterations in reconstruction from $10M$ to $20M$ to optimize the performance.

$$\min_{\alpha \in \mathbb{R}^N} \|\alpha\|_1 \text{ subject to } \|\Phi\Psi\alpha - Y\|_2 \leq \sigma. \tag{13}$$

The boxplots in Fig. 7 show the PRD^* performance for the AD-Q6 and SD-Q6 approaches at varying *CR* and *SNR* levels

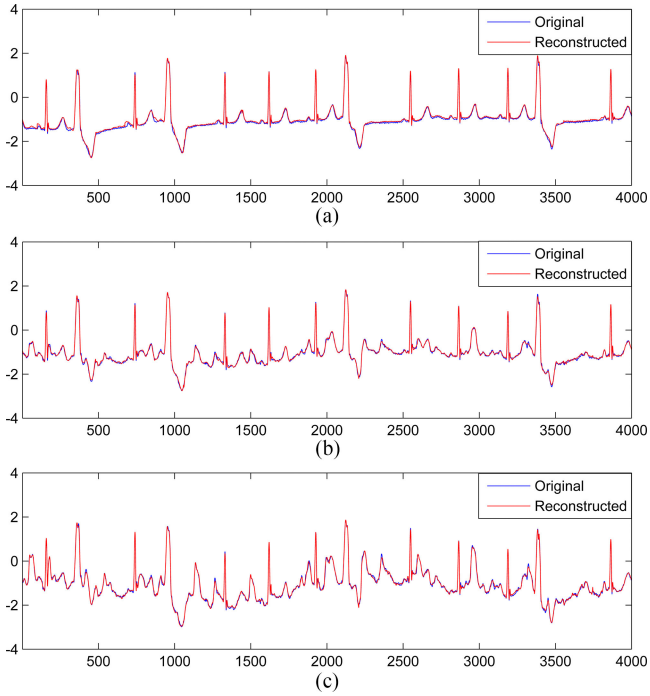

Fig. 6. Examples of three original and reconstructed signals from record 119 for different levels of *SNR*. The original signals are illustrated in blue and the reconstructed signals are in red. (a) shows an original clean signal and a reconstructed signal with a PRD^* of 9.3% at a *CR* of 10.97, (b) shows a signal with a *SNR* of 18 dB reconstructed with a PRD^* of 7.12% at a *CR* of 10.24, and (c) shows a signal with a *SNR* of 12 dB reconstructed with a PRD^* of 6.81% at a *CR* of 9.54.

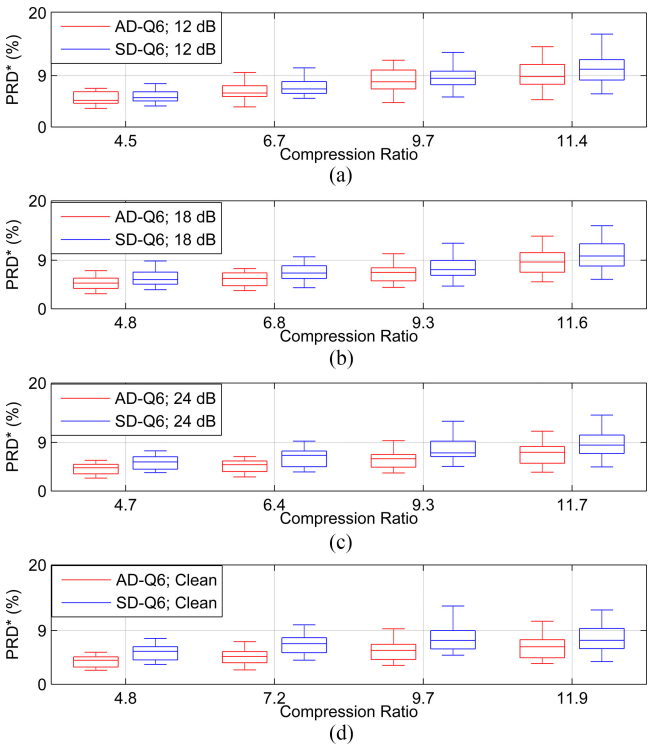

Fig. 7. Boxplots of the PRD^* of AD-Q6 and SD-Q6 tested at different *SNR* levels for approximately equal *CR*s. The performance at (a) 12 dB, (b) 18 dB, (c) 24 dB, and (d) clean signals are illustrated.

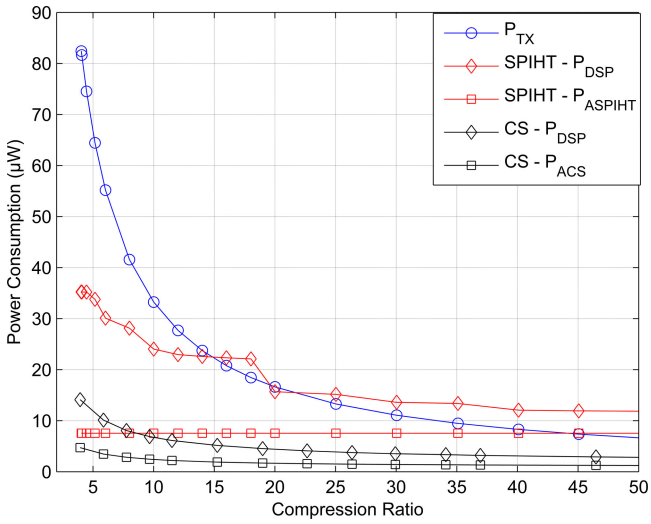

Fig. 8. Power profiles of individual components for each compression algorithm. The power consumption of each process is shown for SPIHT and CS. Symbols are defined in Section IV.

TABLE II
AVERAGE CLOCK CYCLES PER 1 S FOR EACH OPERATION

	CR	DWT	SPIHT coding	P_{DSP} (μW)
SPIHT	2	49034	244563	35.2
	5	49034	232510	34.1
	10	49034	151287	24.0
	20	49034	81680	15.7
	N/M	RR and Huffman coding	Quantization	P_{DSP} (μW)
CS	2	20717	96493	14
	5	8212	48980	6.8
	10	3990	33680	4.5
	20	1879	24699	3.1

averaged over each record. There are two important conclusions about the AD algorithm from Fig. 7. First, the introduction of noise (muscle, electrode, and baseline wander artifacts) does not significantly impact the performance of the AD-Q6 method. While the performance of the AD-Q6 decreases slightly, even at a significant noise corruption level of 12 dB, the algorithm maintains worthwhile performance. For example, up to a *CR* of 11.7, the mean PRD^* value is below the desired 9% for all noise levels with AD-Q6. Second, the ability of AD-Q6 to provide superior performance over SD-Q6 for increasing *SNR* levels is important. The AD-Q6 implementation outperforms the SD-Q6 at each tested *CR*. It is important to note that the AD algorithm maintains improved performance over the SD approach, and the implementation is robust to the presence of the noise related artifacts and electrode motion in reconstruction to demonstrate the full potential of the method for implementation in low-power BANs.

B. Power Profiles of CS and SPIHT

Each of the symbols used in the upcoming Fig. 8, Tables II and III have been previously defined in Section IV. Fig. 8 illustrates the power consumption of the three algorithm operations (sampling, compression, and transmission) for CS and SPIHT at varying *CR*s (note the CS values apply to both SD and AD approaches). The impact of wireless transmission is significant for both algorithms particularly at the lower *CR*s. With regard to SPIHT, at *CR*s beyond 15, P_{DSP} consumes the most power. In fact, the most significant difference between the two algorithms is P_{DSP}. Despite the *AEC* of SPIHT coding decreasing for an increasing *CR*, the DWT element remains constant irrespective of *CR*, ensuring that the drop-off in P_{DSP} is gradual. In contrast, with CS, each of the quantization, Huffman coding and redundancy removal processes decrease in complexity as the number of measurements is reduced. The average clock cycles and power dissipation of each operation at varying *CR*s are shown in Table II, assuming a Blackfin BF537 platform implementation.

TABLE III
ACQUISITION POWER PROFILES FOR SPIHT AND CS

	N/M	P_{MIX} (μW)	P_{INT} (nW)	P_{ADC} (μW)	$P_{\mathrm{ACS}}/P_{\mathrm{ASPIHT}}$ (μW)
SPIHT	–	–	–	7.55	7.55
CS	2	0.95	0.04	3.77	4.73
	5	0.95	0.04	1.51	2.46
	10	0.95	0.04	0.75	1.70
	20	0.95	0.04	0.37	1.33

The acquisition power profiles for each algorithm are also shown in more detail in Table III. SPIHT consumes 7.55 μW during signal acquisition (constant, as Nyquist sampling is used). At a *CR* of 2, CS consumes 4.73 μW and P_{ACS} decreases as compression increases. This is due to a reduction in the number of measurements (*M*) required which reduces P_{ADC}.

C. Overall System Power Consumption

This section compares the AD approach with the MMB approaches, BSBL and SPIHT in terms of overall system power consumption. The ECG signals in the MMB and BSBL implementations in [6] are acquired and compressed using the redundancy removal, quantization, and Huffman encoding techniques described in this paper, and therefore, there is consistency in the comparison. As AD-Q6 was shown to outperform the existing CS approaches in terms of *PRD*, ultimately leading to a reduction in wireless transmission costs, as expected Fig. 9 shows that it outperforms other CS approaches in terms of overall power consumption. SPIHT has the advantage of the minimum cost of wireless transmission, however, the costs associated with acquisition and in particular digital signal compression significantly impact on its performance from a power perspective.

For all *PRD* values considered, AD outperforms the other existing CS techniques. For *PRD* values $> 3\%$, AD-Q6 is the best performing algorithm. However, SPIHT performs best in terms of power consumption for *PRD*s less than 3%. The decline in reconstruction quality for increasing *CR*s is sharper for the MMB and BSBL techniques and SPIHT outperforms MMB-CoSAMP and BSBL at all *PRD*s shown despite the advantages

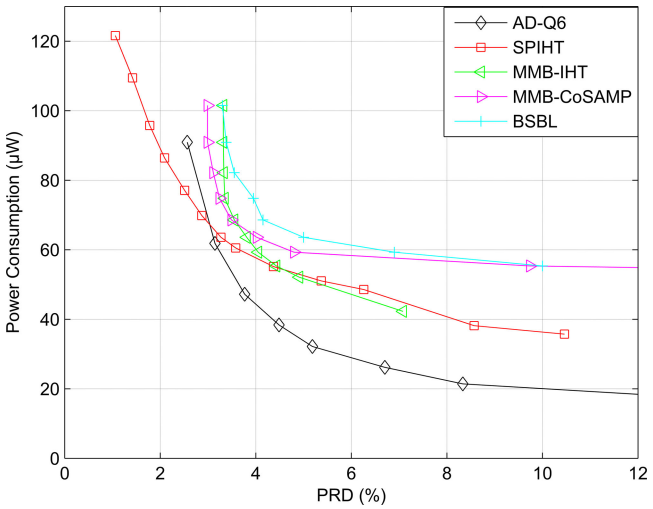

Fig. 9. Total system power profiles of the AD-Q6 implementation, SPIHT, MMB-IHT, MMB-CoSAMP, and BSBL for increasing *PRD* value.

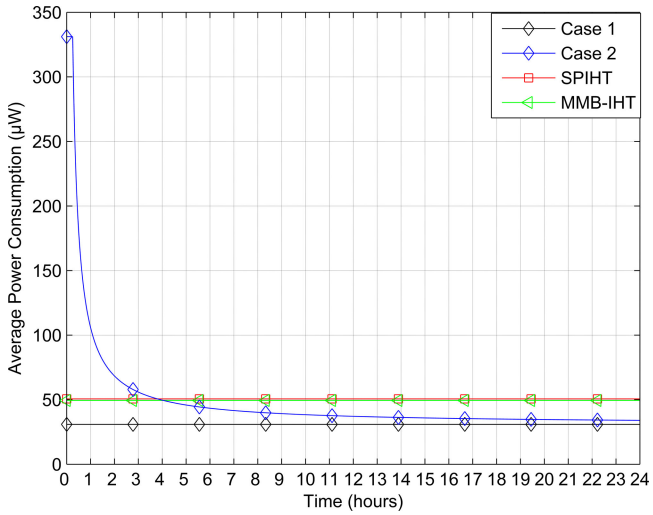

Fig. 10. Comparison of two use cases presented with MMB-IHT and SPIHT over various time durations at an average *PRD* of 5.5%.

in lower power sampling and compression operations. For *PRD* values $> 4.5\%$, MMB-IHT outperforms SPIHT for the *PRD* range shown. It is clear the performance of the AD is superior to the CS techniques tested and this appears to increase as the level of *PRD* increases.

VI. Discussion and Use Case

The main difference between the proposed CS implementation and the existing CS approaches in the literature is that while existing techniques focus on exploiting the structure of the ECG wavelet coefficients, the proposed approach leverages sparsity in reconstruction. The MMB methods exploit knowledge of signal structures and dependences that form across the significant coefficients in different subbands. On the other hand, the BSBL focuses on the interblock structure that exists in the different wavelet decomposition levels of the coefficients. While the most recent high-performing CS techniques demonstrate good reconstruction quality, far superior to the traditional wavelet basis approaches, the combination of the overcomplete patient specific dictionaries and the AD framework ensure the proposed CS architecture can outperform these CS techniques. The AD algorithm allows for superior reconstruction qualities at all *CR*s, but in particular as the *CR* increases the proposed technique is more robust than current CS approaches.

A practical consideration of the AD technique is the requirement for the collection of data for a training phase. Here, we present two use case scenarios for training and analyze the effects on long-term monitoring by estimating the average power consumption over various time periods. Case 1 includes the ideal scenario where training is performed in a clinical environment prior to implementation, adding no power costs to the BAN. Case 2 is the scenario where training is performed on the device itself. The architecture considered in this paper requires a training phase involving the collection of 15 minutes of ECG data. Therefore, Case 2 assumes Nyquist rate sampling for 15 minutes prior to the proposed AD implementation being employed. For comparison purposes, the two use cases will be compared with the MMB-IHT algorithm and SPIHT. It should be noted the MMB approaches utilize Huffman dictionaries in their implementation that require offline creation. However, this is not included in our analysis as training periods are not specified in [6] and [11] and we assume straightforward implementation of the MMB-IHT technique. Similarly, there is no requirement for a training period for SPIHT so the average power consumption stays constant in that case. At a *CR* of 14.8, the AD-Q6 method achieves an average PRD^* of 9% (deemed acceptable for clinical inspection in [33]) and *PRD* of 5.5%. As only average *PRD* (rather than PRD^*) values for were reported MMB-IHT [11] (around the target PRD^*), a *PRD* of 5.5% will be considered the operating point for this use case analysis. At the target *PRD* of 5.5%, AD-Q6 consumes 30.9 μW, SPIHT consumes 50.65 μW, and MMB-IHT consumes 49.4 μW.

Significantly the results in Fig. 10 demonstrate the effects of the additional power consumption used in training are minimal in applications where long-term monitoring is required. The average power consumption of Case 2 closes in on the ideal Case 1 average power as time elapses. From a period of approximately 3 hours and 45 minutes, our estimations suggest Case 2 outperforms the SPIHT approach in terms of average power consumption. It takes approximately 4 hours for the power consumption of Case 2 to be lower than the MMB-IHT implementation. However, once this once-off training phase is complete and sufficient monitoring time has passed the efficiency of Case 2 compared to MMB-IHT and SPIHT continually increases due to the achievable *CR* and low complexity sampling and compression as shown by Fig. 8. This analysis supports the advantages of the proposed approach to reduce power consumption, compared to both SPIHT and existing CS algorithms.

VII. Conclusion

In this paper, we have proposed a novel reconstruction framework for CS-based ECG compression. More specifically,

by combining DL with CS, we exploit knowledge of signal properties based around the prominent QRS complex in order to improve signal reconstruction quality. An important aim of the proposed algorithm was to improve upon existing CS approaches in terms of the tradeoff between *CR* and distortion, and moreover, to reduce the gap in performance between CS and SPIHT, a state-of-the-art transform-based compression algorithm. A further aim was to demonstrate superior performance for the proposed approach compared to SPIHT, in terms of system power consumption. The results validate the potential of the proposed framework as it outperforms i) existing CS techniques in terms of the *PRD* versus *CR* tradeoff and ii) existing CS techniques and SPIHT in terms of power consumption for all *CR*s tested. In particular, the comparison with SPIHT shows a promising boost in CS performance relative to current CS implementations in terms of signal fidelity. The potential of CS for low-energy implementations in wireless BANs has been previously established and the power analysis presented in this paper validates the potential for CS methods, in particular, the proposed AD technique, in ECG compression applications.

References

[1] H. Cao, V. Leung, C. Chow, and H. Chan, "Enabling technologies for wireless body area networks: A survey and outlook," *IEEE Commun. Mag.*, vol. 47, no. 12, pp. 84–93, Dec. 2009.

[2] T. Ma, P. L. Shrestha, M. Hempel, D. Peng, H. Sharif, and H-H. Chen, "Assurance of energy efficiency and data security for ECG transmission in BASNs," *IEEE Trans. Biomed. Eng.*, vol. 59, no. 4, pp. 1041–1048, Apr. 2012.

[3] E. J. Candes, J. Romberg, and T. Tao, "Robust uncertainty principles: Exact signal reconstruction from highly incomplete frequency information," *IEEE Trans. Inf. Theory*, vol. 52, no. 2, pp. 489–509, Feb. 2006.

[4] E. J. Candes and T. Tao, "Near-optimal signal recovery from random projections: Universal encoding strategies?" *IEEE Trans. Inf. Theory*, vol. 52, no. 12, pp. 5406–5425, Dec. 2006.

[5] D. L. Donoho, "Compressed sensing," *IEEE Trans. Inf. Theory*, vol. 52, no. 4, pp. 1289–1306, Apr. 2006.

[6] H. Mamaghanian, N. Khaled, D. Atienza, and P. Vandergheynst, "Compressed sensing for real-time energy-efficient ECG compression on wireless body sensor nodes," *IEEE Trans. Biomed. Eng.*, vol. 58, no. 9, pp. 2456–2466, Sep. 2011.

[7] H. Mamaghanian, N. Khaled, D. Atienza, and P. Vandergheynst, "Design and exploration of low-power analog to information conversion based on compressed sensing," *IEEE J. Emerging Sel. Topics Circuits Syst.*, vol. 2, no. 3, pp. 493–501, Sep. 2012.

[8] M. L. Hilton, "Wavelet and wavelet packet compression of electrocardiograms," *IEEE Trans. Biomed. Eng.*, vol. 44, no. 5, pp. 394–402, May 1997.

[9] A. Said and W. A. Pearlman, "A new, fast, and efficient image codec based on set partitioning in hierarchical trees," *IEEE Trans. Circuits Syst. Video Technol.*, vol. 6, no. 3, pp. 243–250, Jun. 1996.

[10] Z. Zhang, T-P. Jung, S. Makeig, and B. D. Rao, "Compressed sensing for energy-efficient wireless telemonitoring of noninvasive fetal ECG via block sparse Bayesian learning," *IEEE Trans. Biomed. Eng.*, vol. 60, no. 2, pp. 300–309, Feb. 2013.

[11] L. F. Polania, R. E. Carrillo, M. Blanco-Velasco, and K. E. Barner, "Exploiting prior knowledge in compressed sensing wireless ECG systems," *IEEE J. Biomed. Health Informat.*, vol. 19, no. 2, pp. 508–519, Mar. 2015.

[12] D. Craven, B. McGinley, L. Kilmartin, M. Glavin, and E. Jones, "Impact of compressed sensing on clinically relevant metrics for ambulatory ECG monitoring," *Electron. Lett.*, vol. 51, pp. 323–325, 2015.

[13] D. Craven, B. McGinley, L. Kilmartin, M. Glavin, and E. Jones, "Compressed sensing for bioelectric signals: A review," *IEEE J. Biomed. Health Informat.*, vol. 19, no. 2, pp. 529–540, Mar. 2015.

[14] Analog Devices Blackfin DSP - ADSP-BF537. (2014). [Online]. Available: http://www.analog.com/en/processors-dsp/blackfin/adsp-bf537/products/product.html

[15] Texas Instruments Bluetooth Low-Energy System-on-Chip - CC2540. (2015). [Online]. Available: http://www.ti.com/product/cc2540

[16] E. J. Candes and M. B. Wakin, "An introduction to compressive sampling," *IEEE Signal Process. Mag.*, vol. 25, no. 2, pp. 21–30, Mar. 2008.

[17] S. S. Chen, D. L. Donoho, and M. A. Saunders, "Atomic decomposition by basis pursuit," *J. Sci. Comput.*, vol. 20, pp. 33–61, 1999.

[18] J. A. Tropp, "Just relax: Convex programming methods for identifying sparse signals in noise," *IEEE Trans. Inform. Theory*, vol. 52, no. 3, pp. 1030–1051, Mar. 2006.

[19] L. F. Polania and K. E. Barner, "Multi-scale dictionary learning for compressive sensing ECG," in *Proc. IEEE Digital Signal Process. Signal Process. Edu. Meet.*, 2013, pp. 36–41.

[20] M. Aharon, M. Elad and A. Bruckstein, "K-SVD: An algorithm for designing overcomplete dictionaries for sparse representation," *IEEE Trans. Signal Process.*, vol. 54, no. 11, pp. 4311–4322, Nov. 2006.

[21] Y. Juhwan, S. Becker, M. Monge, M. Loh, E. Candes, and A. Emami-Neyestanak, "Design and implementation of a fully integrated compressed-sensing signal acquisition system," in *IEEE Int. Conf. Acoust., Speech Signal Process.*, 2012, pp. 5325–5328.

[22] MIT-BIH Arrhythmia Database. (2000). [Online]. Available: http://www.physionet.org/physiobank/database/mitdb./

[23] Z. Lu, D. Y. Kim, and W. A. Pearlman, "Wavelet compression of ECG signals by the set partitioning in hierarchical trees algorithm," *IEEE Trans. Biomed. Eng.*, vol. 47, no. 7, pp. 849–856, Jul. 2000.

[24] MIT-BIH Arrhythmia Database Directory. (2000). [Online]. Available: http://physionet.org/physiobank/database/html/mitdbdir/records.htm

[25] MIT-BIH Noise Stress Test Database. (2000). [Online]. Available: http://www.physionet.org/physiobank/database/nstdb./

[26] Z. Zhang, T. Jung, S. Makeig, and B. Rao, "Compressed Sensing of EEG for wireless telemonitoring with low energy consumption and inexpensive hardware," *IEEE Trans. Biomed. Eng.*, vol. 60, no. 1, pp. 221–224, Jan. 2013.

[27] M. E. Angelopoulou, K. Masselos, P. Y. K. Cheung, and Y. Andreopoulos, "Implementation and comparison of the 5/3 lifting 2D discrete wavelet transform computation schedules on FPGAs," *J. Signal Process. Syst.*, vol. 51, pp. 3–21, 2008.

[28] K. Andra, C. Chakrabarti, and T. Acharya, "A VLSI architecture for lifting-based forward and inverse wavelet transform," *IEEE Trans. Signal Process.*, vol. 50, no. 4, pp. 966–977, Apr. 2002.

[29] F. Chen, A. P. Chandrakasan, and V. M. Stojanovic, "Design and analysis of a hardware-efficient compressed sensing architecture for data compression in wireless sensors," *IEEE J. Solid-State Circuits*, vol. 47, no. 3, pp. 744–756, Mar. 2012.

[30] B. Murmann. (2014). ADC Performance Survey 1997–2014. [Online]. Available: http://web.stanford.edu/~murmann/adcsurvey.html

[31] Estimating Power for ADSP-BF534/BF536/BF537 Blackfin Processors. (2014). [Online]. Available: http://www.analog.com/static/imported-files/application_notes/EE-297.Rev.3.11.07.pdf

[32] M. Siekkinen, M. Hiienkari, J. K. Nurminen, and J. Nieminen, "How low energy is bluetooth low energy? Comparative measurements with ZigBee/802.15.4," in Proc. IEEE Wireless Commun. Netw. Conf. Workshops, 2012, pp. 232–237.

[33] Y. Zigel, A. Cohen, and A. Katz, "The weighted diagnostic distortion (WDD) measure for ECG signal compression," *IEEE Trans. Biomed. Eng.*, vol. 47, no. 11, pp. 1422–1430, Nov. 2000.

[34] E. van den Berg and M. P. Friedlander, "Probing the Pareto frontier for basis pursuit solutions," *SIAM J. Sci. Comput.*, vol. 31, pp. 890–912, 2009.

Authors' photographs and biographies not available at the time of publication.